Thermal degradation kinetics of polyvinyl chloride in presence of zinc oxide

Sanad Altarawneh[1],* Mohammad Al-Harahsheh[2], Chris Dodds[1], Adam Buttress[1], Sam Kingman[1]

[1] Faculty of Engineering, University of Nottingham, Nottingham, NG7 2RD, UK

[2] Chemical Engineering Department, Jordan University of Science and Technology, Irbid, 22110, Jordan

*corresponding author

Sanad.altarawneh@nottingham.ac.uk

Abstract

This work investigates the degradation kinetics and the pyrolysis behaviour of Poly (vinyl chloride) (PVC) and its mixture with ZnO using thermogravimetric analysis under an inert atmosphere. The investigation was carried out due to the increased interest in the co-thermal treatment of the hazardous waste electric arc furnace dust (EAFD) which contains significant quantities of ZnO with PVC. The degradation of pure PVC was characterised by three main decomposition stages: PVC de-hydrochlorination (two overlapped stages) and subsequent polyene thermal cracking, while ZnO-PVC mixture (ZPVC) demonstrated four decomposition/volatilisation stages. The Flynn-Wall-Ozawa (FWO), Kissinger-Akahira-Sunose (KAS), and Friedman models were utilised for the extraction of the kinetic parameters. The average activation energy for pure PVC de-hydrochlorination was calculated to be 119.8 ± 12.4 kJ/mol, which changed to 110.6 ± 11.2 kJ/mol when a stoichiometric quantity of ZnO was added to it. The suggested mechanism for the ZPVC de-hydrochlorination starts by chlorine abstraction on ZnO at temperatures well-below 272 °C with an activation energy comparable to that of pure PVC de-hydrochlorination (115.8 kJ/mol). The chlorination of ZnO then yields zinc oxy/hydroxide chloride phases ($Zn_2OCl_2.2H_2O$/β-Zn(OH)Cl) by the reaction between $ZnCl_2$, ZnO and emitted H_2O. These phases then decompose at approximately 222 °C into $ZnCl_2$, ZnO, and H_2O with a relatively low energy barrier of 102.2 kJ/mol. Formed $ZnCl_2$ then lowers the activation energy for the polyene thermal cracking of PVC from 218.4 ± 17.7

(PVC) to 87.3 ± 9.7 kJ/mol (ZPVC) due to the physical contribution of volatilisation to the overall mass loss.

Keywords: PVC, ZnO, polymer degradation, pyrolysis, TGA, non-isothermal kinetics

1. Introduction

Electric arc furnace dust (EAFD) is globally considered a major hazardous waste material which is generated from steel manufacturing in electric arc furnaces (EAFs) [1]. Between 15 and 20 kg of EAFD is generated for every ton of recycled steel [2]. Each year approximately 8 million tons of EAFD are generated and this is predicted to increase to a minimum of 18 million tons/year by 2050 [3]. This alarming production rate with the absence of a sustainable recycling route poses a great challenge to environmental engineers. The major part of the feed supplied to EAFs is steel scrap [4] and since a significant portion of this scrap is galvanised, high zinc concentrations are usually seen in EAFD [2, 5-7]. This, in turn, rendered EAFD as a potential secondary source for zinc. The conventional methods suggested in literature for the extraction of zinc from EAFD can be categorised into hydrometallurgical [2, 8-11] and pyrometallurgical [12-14]. The former approach, whilst typically lower in energy consumption and more environmentally benign, suffers from incomplete extraction [15-17], harshness of the leaching medium [16], and poor selectivity [16, 18]. Pyrometallurgical treatments, have found industrial scale applications such as the Waelz kiln. However, this approach is highly energy intensive (furnace operates above 1000 °C) and environmentally harmful and therefore requires complicated gas/dust filtration systems downstream [1].

Parallel to accumulations of EAFD, polyvinyl chloride (PVC) is another waste stream generated in huge quantities. This material is one of the most widely used plastics and it finds use in a diverse range of applications including construction, packaging, piping, cable insulation, and medical applications [19]. The global production and consumption capacity of PVC in 2013 was 61 and 38.5 million tons [20] with an estimated annual rise in demand of 3.2% until 2021 [21]. Using this percentage (3.2%/year), today, a consumption rate of about 49.5 million tons is expected. Consequently, it has become increasingly important to address the associated PVC waste streams which arise at the end of the life cycle of these various

products. A Landfill strategy was the most prevalent disposal route, but over time, it has become an obsolete option due to the decreased number of landfilling sites [22] and the associated environmental burden. In addition, the high stability of PVC in landfills [23] requires vast dumping areas which significantly increase the costs of landfilling. An alternative to landfilling is the pyrolysis of PVC. This treatment, however, yields harmful emissions such as hydrogen chloride (HCl) gas and chlorinated hydrocarbons such as polychlorinated dibenzo-p-dioxins (PCDDs) and polychlorinated dibenzofurans (PCDFs) [24, 25].

Recently, there has been a growing interest among researchers towards the co-thermal treatment of waste EAFD with halogenated plastics such as PVC [1, 5, 7, 26, 27]. The metal oxides present in EAFD proved to have remarkable fixing ability of the emissions generated from the pyrolysis of PVC, especially HCl [7, 22, 27]. Masuda et al. [28] studied the HCl fixing ability of eight metal oxides including ZnO. It was concluded that ZnO is capable of capturing 51% of the initial chlorine content of PVC when pyrolysed at a temperature of 400 °C. Likewise, ZnO resulted in a significant reduction in the yield of chlorobenzene; one of the main precursors of PCDD/Fs [28]. Ballistreri et al. [29] studied the effect of eight metal oxides on the decomposition of PVC among which ZnO showed a very powerful supressing effect on the emission of aromatic species. In the same study, the formation of volatilised $ZnCl_2$ was detected by a mass spectrometer [29]. Zhang et al. [30], studied the decomposition of PVC in the presence of ZnO, $ZnFe_2O_4$, and Fe_2O_3 and concluded that the degradation of PVC proceeded at a lower temperature in the presence of ZnO. The chlorine fixation on ZnO was also confirmed by the detection of H_2O fragments evolved from chlorination using a mass spectrometer [30].

Since the interest in the co-thermal treatment of waste EAFD and waste PVC grew for the purpose of zinc extraction, and since a major portion of zinc in EAFD is present in the form of ZnO, a comprehensive kinetics study on the effect of ZnO on the decomposition of PVC has

become necessary in order to predict reaction rates at different holding temperatures and conversions. This also helps in understanding the underpinning reaction mechanisms by means of comparing the activation energy and the reaction mechanism $f(\alpha)$ for ZnO-PVC (ZPVC) mixture and pure PVC. In this study, we present a complete non-isothermal kinetic study of pure PVC and ZPVC mixtures in the temperature window 25 – 900 °C and under inert environment. From this, the activation energy, the frequency factor, and the reaction mechanism $f(\alpha)$ can be extracted using different iso-conversional kinetics models -namely the well-known FWO, KAS, and Friedman [31-35] along with a linear fitting method. Pyrolysis products of ZPVC mixture were also identified using X-Ray diffraction (XRD) and Scanning electron microscopy (SEM) techniques to support the validity of the derived mechanisms.

2. Materials and method

2.1 Thermogravimetric analysis and differential scanning calorimetry

The ZnO used in this work was purchased from Fisher Scientific with a purity of 99.999%, and powdered PVC was obtained from Sigma-Aldrich. A stoichiometric mixture of ZnO and PVC (ZPVC) was prepared based on the stoichiometric amount of HCl in the PVC monomer; this produced a mixture containing 39.4 wt% ZnO. Before mixing, ZnO powder was finely ground using pestle and mortar to increase the homogeneity of the mixture and to increase the contact surface area for the chemical reaction (see Figures S1 and S2 in the supplementary material). The ZPVC mixture was then tumbled for 15 minutes in a glass vial containing stainless steel balls in order to prevent particles agglomeration and make sure the particle size is uniform throughout. An empty ceramic sample holder was first exposed to the thermal analysis to produce a baseline for the heat flow signal. A sample of about 10 mg of pure PVC and ZPVC mixture were then exposed to thermal analysis using a simultaneous differential scanning calorimetry (DSC) and Thermogravimetric Analysis (TGA) instrument (SDT Q600). The

thermal analysis was performed at three different heating rates (10, 30, and 50 K/min) in the temperature window of 25 – 900 °C and under a nitrogen flow of 100 mL/min.

2.2 Pyrolysis of ZPVC mixture

A sample with a mass of 0.3 g (for 200 and 230 °C) and 0.5 g (for 370 °C) of ZPVC mixture was loaded into a 4 mm quartz tube. The usage of two different masses for different pyrolysis temperatures was because of the different mass loss at different temperatures. This, in turn, ensures that a comparable amount of powder residue was obtained after the pyrolysis. The tube was connected from one end to high purity nitrogen (99.9992%) to purge the ZPVC mixture at a rate of ~ 5 mL/min, and the other end was vented into an extraction system. The powder was surrounded from the top and bottom with ceramic fibre to prevent it from fluidising. The bottom ceramic fibre also acted as a gas distributor (to distribute the gas evenly through the powder). Prior to heating, the system was purged with nitrogen for at least 15 minutes to confirm that the reactants are completely surrounded with a nitrogen blanket. The quartz tube was then inserted vertically into a tube furnace. Three pyrolysis runs were performed at three different temperatures of 200, 230 and 370 °C and the mixture was held at these temperatures for 30 minutes. Products from each run were collected in a vial, purged with nitrogen, and stored in a desiccator for characterisation.

2.3 Scanning electron microscopy analysis

A FEI Quanta600 MLA scanning electron microscope (SEM) coupled with Energy Dispersive Spectroscopy (EDS) was used for the morphological and elemental analysis of the powder before and after pyrolysis. A spot size of 4.5 and an accelerating voltage of 15000 kV were used during the analysis. To enhance the electrical conductivity of the powder and avoid charging during the analysis, powders were carbon coated.

2.4 X-ray diffraction analysis

Residues generated from the pyrolysis were subjected to X-ray diffraction (XRD) for mineralogical identification of products. To minimise the effect of moisture on the materials, powders on the sample holder were covered from the top with a piece of tape to prevent fresh air from being in contact with it. A Bruker D8 Advance with a LYNXEYE 2D detector and a Cu kα source was used for the mineralogical analysis. The instrument was operated at a current and voltage of 40 mA and 40 kV, respectively. Pyrolysis residues were scanned in the 2θ range 5 – 90° with a step size of 0.02° and a scan rate of 1.7 sec/step while pure ZnO was scanned at 0.1 sec/step due to its high purity and non-noisy signal. Data was interpreted using QualX 2.0 [36] and DIFFRAC.EVA V5.2 softwares which use COD and PDF-2 databases, respectively.

3. Non-isothermal kinetics model

3.1 General rate equation

The rate of solid decomposition (r_A) can be given by the product of the temperature dependent rate constant $k(T)$ and the temperature independent conversion function $f(\alpha)$ (reaction model):

$$r_A = \frac{d\alpha}{dt} = k(T).f(\alpha) \quad (1)$$

In which α is the degree of conversion and $\frac{d\alpha}{dt}$ is its derivative with respect to time.

The mathematical expression used for the $f(\alpha)$ function depends on the controlling mechanism of the reaction. An empirical model introduced by Šesták and Berggren [37] for the form of $f(\alpha)$ can be written as:

$$f(\alpha) = \alpha^m(1 - \alpha)^n[-\ln(1-\alpha)]^p \quad (2)$$

Where different combinations of m, n, and p result in different reaction models [38]. The conversion α is calculated from the wt% data produced from the TGA profile as follows:

$$\alpha = \frac{W_o - W}{W_o - W_f} \quad (3)$$

Where W is the wt% at time t, W_o is the initial wt% and W_f is the final wt%. The rate constant in Equation 1 depends on temperature according to the Arrhenius function:

$$k(T) = A.e^{\frac{-E}{RT}} \quad (4)$$

Where A is the temperature independent frequency factor given in min^{-1}, E is the activation energy in J/mol, R is the universal gas constant (8.314 J/mol.K) and T is the absolute temperature in K. Combining Equations 1 and 4 and multiplying both sides with the reciprocal of the heating rate $\left(\frac{1}{\beta} = \frac{dt}{dT}\right)$ yields the following equation:

$$\frac{r_A}{\beta} = \frac{d\alpha}{dT} = \frac{A}{\beta} e^{\frac{-E}{RT}}.f(\alpha) \quad (5)$$

Equation 5 is the derivative form of the rate equation. Rearranging and integrating both sides yields the integral form of the rate equation:

$$g(\alpha) = \int_0^{\alpha} \frac{d\alpha}{f(\alpha)} = \frac{A}{\beta} \int_{T_o}^{T} e^{\frac{-E}{RT}} dT \quad (6)$$

In which T_o corresponds to a conversion of zero. The right-hand side of Equation 6 has no analytical solution [39]. Thus, different methods were developed to either utilise the differential form (Equation 5) or use estimations for the temperature integral in Equation 6 to calculate the activation energy and the frequency factor. Among many kinetics methods, the iso-conversional technique allows for a reliable prediction of the kinetic parameters [40, 41].

3.2 Model-Free methods

3.2.1 Calculation of the activation energy

The Flynn-Wall-Ozawa (FWO) method [33, 34] uses the Doyle [42] approximation of the integration in Equation 6 for the calculation of the kinetic parameters. Their model can be written as follows:

$$ln\beta_i = ln\left(\frac{A_\alpha E_\alpha}{g(\alpha)R}\right) - 5.331 - 1.052\frac{E_\alpha}{RT_{\alpha i}} \quad (7)$$

For a specific value of conversion (α), three different temperatures are obtained for three thermograms at three different heating rates. A plot of $ln\beta_i$ versus $\frac{1}{T_{\alpha i}}$ should produce a straight line with a slope of $-1.052\frac{E_\alpha}{R}$ from which the apparent activation energy is obtained.

Kissinger-Akahira-Sunose (KAS) [31, 35] is another method that uses the integral form of the rate equation for the calculation of the kinetic parameters. Their model can be written according to the following equation:

$$ln\left(\frac{\beta_i}{T^2{}_{\alpha i}}\right) = ln\left(\frac{A_\alpha R}{E_\alpha g(\alpha)}\right) - \frac{E_\alpha}{RT_{\alpha i}} \quad (8)$$

Likewise, a plot of $ln\left(\frac{\beta_i}{T^2{}_{\alpha i}}\right)$ against $\frac{1}{T_{\alpha i}}$ at a constant conversion for three different thermograms at three different heating rates must yield a straight line with a slope of $-\frac{E_\alpha}{R}$.

Friedman method [32] uses the differential form of the rate equation. The model can be written as follows:

$$ln\left(\frac{d\alpha}{dt}\right)_i = lnA + lnf(\alpha) - \frac{E_\alpha}{RT_{\alpha i}} \quad (9)$$

A plot of $ln\left(\frac{d\alpha}{dt}\right)_i$ against $\frac{1}{T_{\alpha i}}$ at a constant conversion for three heating rates produces a straight line with a slope of $-\frac{E_\alpha}{R}$.

3.2.2 Calculation of the frequency factor

The extraction of the frequency factor can be achieved using the compensation effect described in Vyazovkin [43]. Fitting the experimental data (Equation 11) using a set of different reaction models generates a set of values of activation energy and frequency factor. The activation energies and frequency factors can then be linearly correlated (see Figure S3 in supplementary material) according to the following Equation [43]:

$$ln(A_i) = aE_i + b \quad (10)$$

Such that a and b are constants obtained from linear regression. Activation energies obtained from the model-free methods can then be inserted into Equation 10 to extract iso-conversional values of $ln\ (A)_\alpha$.

3.3 Prediction of the reaction model

These methods, usually referred to as "iso-conversional" or "model free", are useful when calculating the activation energy, since the exact knowledge of the reaction model "$f(\alpha)$" is not required. Hence, these methods cannot be used to predict the reaction model. The re-arrangement of Equation 5 into Equation 11 allows the prediction of the reaction model $f(\alpha)$ by means of linear fitting of $ln\left(\frac{d\alpha}{dt}.\frac{1}{f(\alpha)}\right)$ against $\frac{1}{T}$:

$$ln\left(\frac{d\alpha}{dt}.\frac{1}{f(\alpha)}\right) = ln(A) - \frac{E}{RT} \quad (11)$$

The criteria followed for this method was that the accepted reaction model is the one that gives the best linearity, and its slope should generate a value of activation energy that is as close as possible to the average value obtained from the Friedman model on the studied conversion range. When possible, the chosen reaction orders were those that generate a meaningful reaction model, rather than random polynomials.

4. Results and Discussion

4.1. TGA/DSC analysis

4.1.1. TGA/DSC analysis of pure PVC

Figure 1 shows the TGA and Differential thermogravimetric (DTG) (derivative mass) profiles for the decomposition of pure PVC at heating rates of 10, 30 and 50 K/min. PVC degradation follows three decomposition stages. The first two stages are overlapped while the third one is well separated.

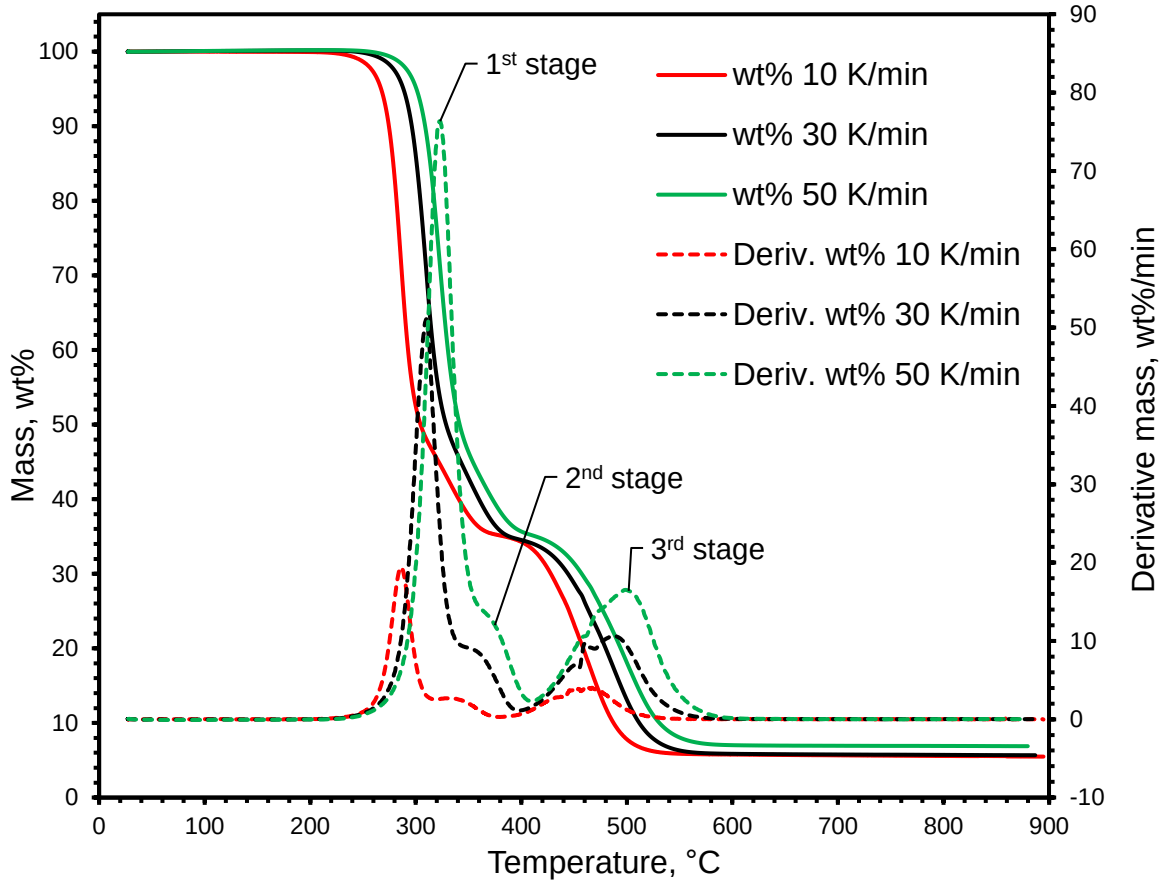

Figure 1: TGA/DTG profiles for PVC decomposition at heating rates of 10, 30, and 50 K/min and under a nitrogen flow of 100 mL/min.

The first two overlapped stages with an onset temperature of 272 °C have an overall mass loss of 65%. This mass loss is assigned to the de-hydrochlorination of the polymer chain and the evolution of hydrogen chloride gas (HCl) [44]. The theoretical HCl content in the PVC monomer is 58.3%. The disparity between 65% and 58.3% was assigned to the emission of volatile aromatic compounds, such as benzene, naphthalene, and anthracene [29]. At the end

of the first two stages, the PVC chain is stripped from its chlorine content and the remaining solid is a conjugated polyene structure [20, 44]. The chemical reaction in the first two stages can be written as follows [45]:

$$(\text{—}CH_2\text{-}CHCl\text{—}CH_2\text{—}CHCl\text{—})_n \rightarrow (\text{—}HC{=}CH\text{—}CH{=}CH\text{—})_n + HCl_{(g)} \quad (12)$$

The third stage with an onset temperature of 423 °C and represented by a mass loss of 29%, is attributed to the thermal cracking of the polymer backbone (polyene structure) into other hydrocarbons such as polyenyl aromatics, alkyl aromatics, and polyaromatics [46]. At the end of the third stage, about 6% of the initial weight remains in the crucible. The pyrolysis residue was reported to be char [1, 29]. Hence, the chemical reaction occurring during the third stage can be written as:

$$(\text{—}HC{=}CH\text{—}CH{=}CH\text{—})_n \rightarrow \text{Char} + \text{Volatile hydrocarbons} \quad (13)$$

Both the de-hydrochlorination (first two stages) and the polyene thermal cracking (third stage) are accompanied by endothermic events as evident from the heat flow signals (peaks 2 and 3 in Figure 2).

4.1.2. TGA/DSC analysis of ZPVC mixture

Figure 3 (a) shows the decomposition of the ZPVC mixture at heating rates of 10, 30, and 50 K/min. The decomposition follows four degradations stages; the first three are overlapped showing a DTG triplet, while the fourth is well separated. The de-hydrochlorination onset temperature for the ZPVC mixture is 214 °C, well-below that of pure PVC (Figure 2).

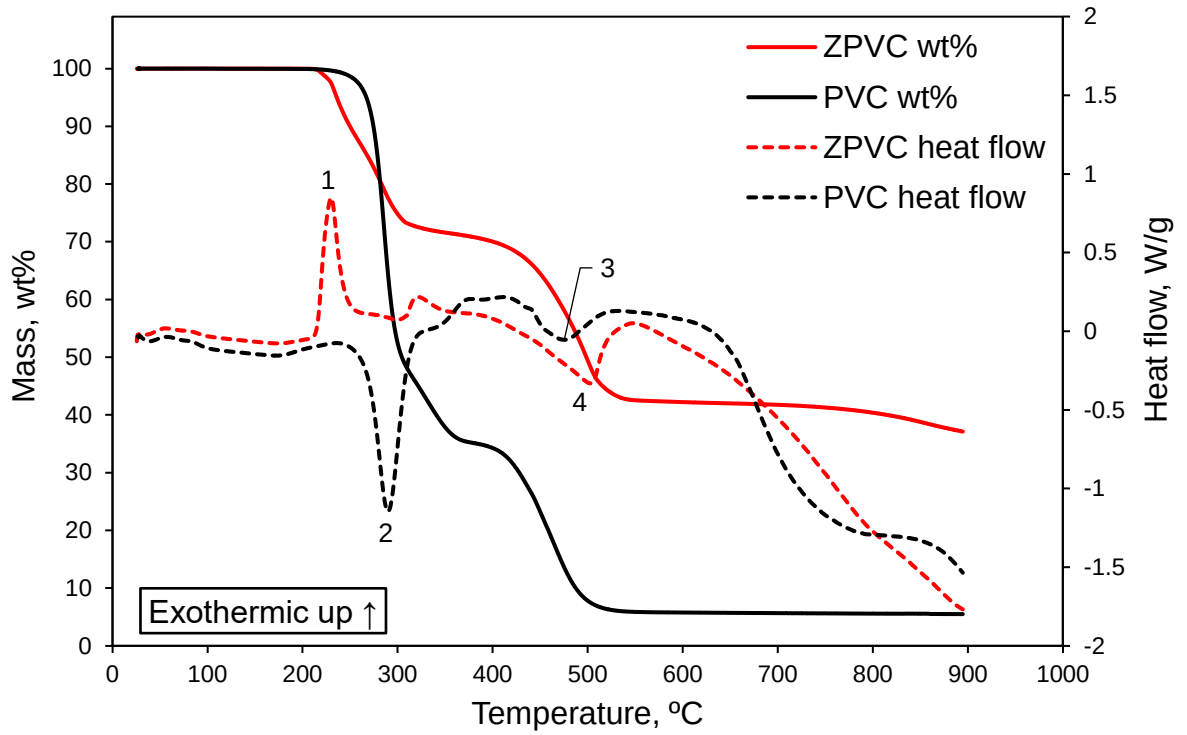

Figure 2: Simultaneous TGA/DSC profiles for PVC and ZPVC mixture at a heating rate of 10 K/min and a nitrogen flow of 100 mL/min (DSC signals can be assigned as follows: 1. ZnO chlorination, 2. PVC de-hydrochlorination, 3. polyene thermal cracking and 4. simultaneous $ZnCl_2$ volatilisation and polyene thermal cracking).

Such behaviour suggests that ZnO can be categorised as an active catalyst for the de-hydrochlorination of PVC changing its initiation pathway. The start of PVC degradation at a lower temperature when mixed with ZnO was also seen in the work from Zhang et al. [30] and Kosuda et al. [47]. The pyrolysis of EAFD-PVC mixture by Al-Harahsheh et al. [1] also showed similar results where the onset temperature significantly decreased when PVC was pyrolysed in presence of EAFD; the latter contained more than 29 wt% zinc with a large portion in the form of ZnO [1, 7].

Figure 3 (a) shows that increasing the heating rate increases the percentage of captured HCl as evident from the lower mass loss at higher heating rates. An estimation of how much HCl was captured by ZnO can be obtained from the mass loss in the first three stages and the knowledge of the initial composition of the mixture. This procedure gives only an estimation since it assumes that the first three stages are only related to HCl evolution (i.e., neglecting organic emissions) and that the chlorination occurs according to Equation 15.

The percentage fixed can be given as follows:

$$\text{Fixed HCl (wt\%)} = \frac{W - W^*}{W' - W^*} \times 100\% \quad (14)$$

Where W^* is the wt% left in crucible if no HCl was captured (64.7%), W' is the wt% left if all HCl was captured (91.3%) and W, as defined earlier, is the actual wt% remaining from the experiment. Using Equation 14, the percentage of HCl captured by ZnO was calculated to be 28.9, 42.6 and 46.3% at 10, 30 and 50 K/min, respectively. These percentages, at high heating rates, are comparable to the HCl fixation values reported by Masuda et al. [28].

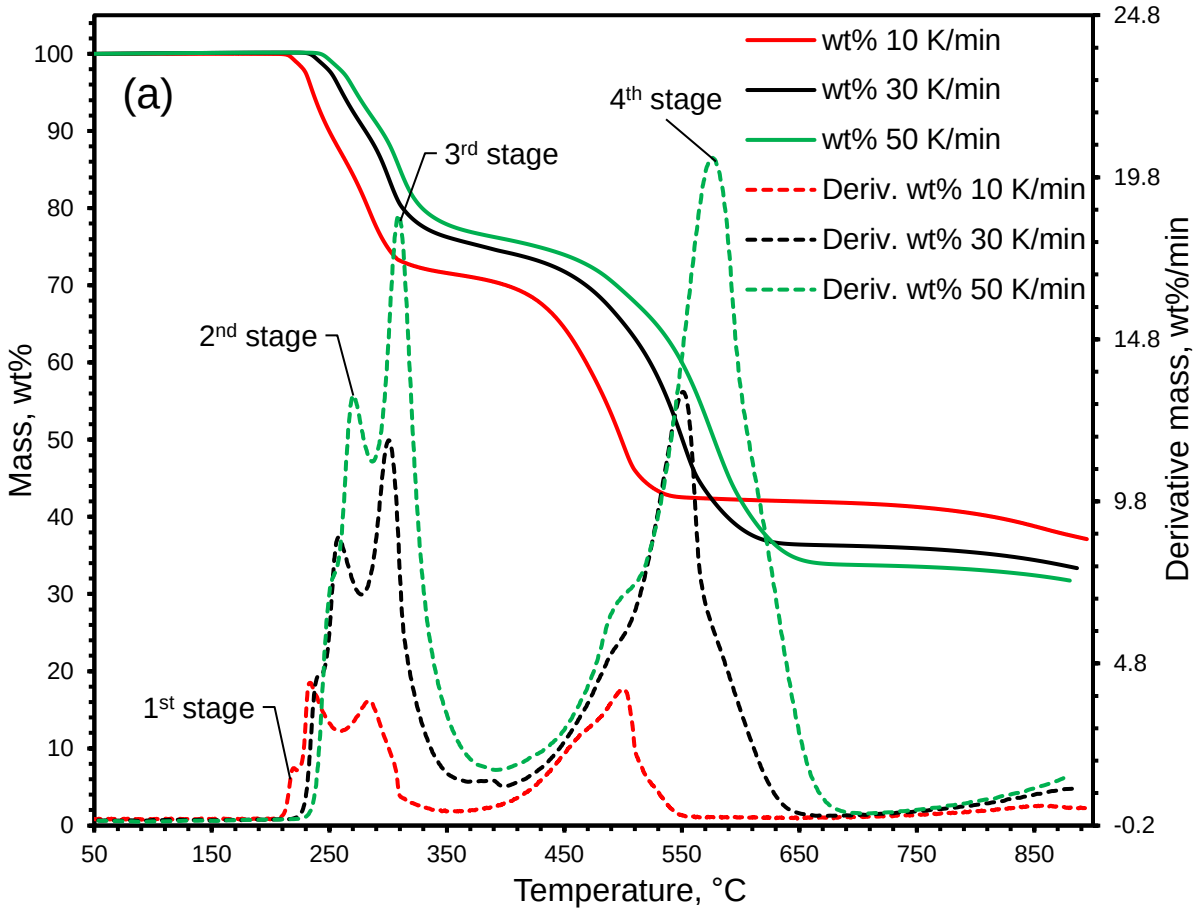

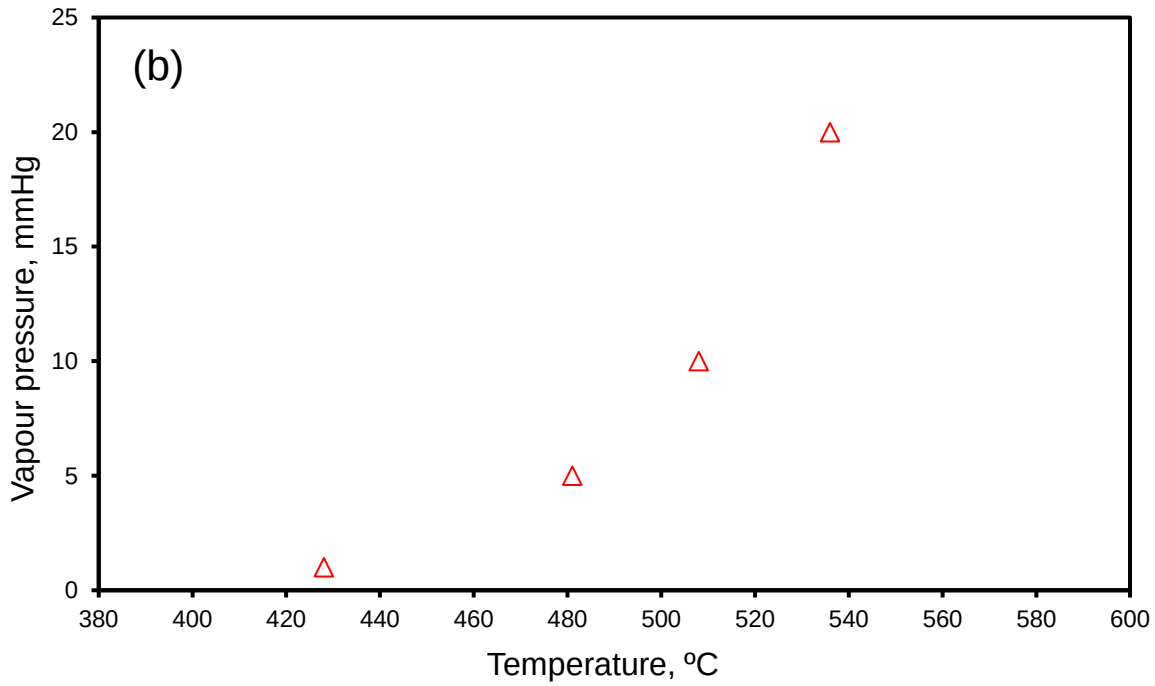

Figure 3: (a) TGA/DTG profiles for the ZPVC mixture (39.4 wt% ZnO) at heating rates of 10, 30 and 50 K/min and under a nitrogen flow of 100 mL/min (b) vapour pressure of $ZnCl_2$ against temperature [48].

In Figure 3 (a), the first two stages may be attributed to the release of H_2O resulting from the chlorination of ZnO [27, 30]. H_2O also evolves from the decomposition of intermediate zinc oxy/hydroxide chloride species as will be shown later. The chlorination of ZnO can be confirmed from the high exothermic peak appearing in the temperature range 210 – 260 °C in Figure 2, which is absent in the case of pure PVC. XRD characterisation of the products generated from the pyrolysis experiments performed at 200, 230 and 370 °C, shows peaks related to β-Zn(OH)Cl, $Zn_2OCl_2.2H_2O$, α-$ZnCl_2$, and $ZnCl_2.1.33H_2O$ (Figure 4). One more phase (Simonkolleite: $Zn_5(OH)_8Cl_2.H_2O$) was reported to form at temperatures 180 – 200 °C by Kosuda et al. [47] which acts as a precursor for the β-Zn(OH)Cl and $Zn_2OCl_2.2H_2O$ phases reported here [49, 50]. Distinguishing whether β-Zn(OH)Cl or $Zn_2OCl_2.2H_2O$ was the formed phase is difficult since both phases have the same 2θ angles. The thermal behaviour of both β-Zn(OH)Cl and $Zn_2OCl_2.2H_2O$ reported in literature [51-53] is very comparable to one another and both agree well with the TGA data reported in Figure 3 (a) as will be discussed later. It is noted that the abundance of the formed chloride species is affected by the temperature at which

287 the pyrolysis takes place. When the pyrolysis temperature was increased from 200 to 230 and
288 370 °C, the intensity of $Zn_2OCl_2.2H_2O$/β-Zn(OH)Cl peaks waned. This drop in intensity was
289 accompanied by the appearance of α-$ZnCl_2$ and $ZnCl_2.1.33H_2O$ peaks at 230 °C and α-$ZnCl_2$
290 peaks at 370 °C. This suggests that $Zn_2OCl_2.2H_2O$/β-Zn(OH)Cl can be considered as
291 intermediate chloride species which decompose into α-$ZnCl_2$, $ZnCl_2.1.33H_2O$, ZnO and H_2O
292 when the temperature increases further. This result is in agreement with the work performed
293 by Ahmed et al. [54]. In their study, a thermo-kinetic model on the dissociative adsorption and
294 reaction of gaseous molecular HCl with ZnO $(10\bar{1}0)$ surface was constructed and the
295 mechanistic pathway of the reactions including all intermediates was reported [54]. The
296 formation of surface zinc chloride on the ZnO crystal and the attachment of hydrogen atom
297 from the HCl molecule with the oxygen on ZnO crystal was also reported. This, in turn, led to
298 the conclusion that a zinc oxychloride intermediate was formed prior to the formation of zinc
299 chloride.

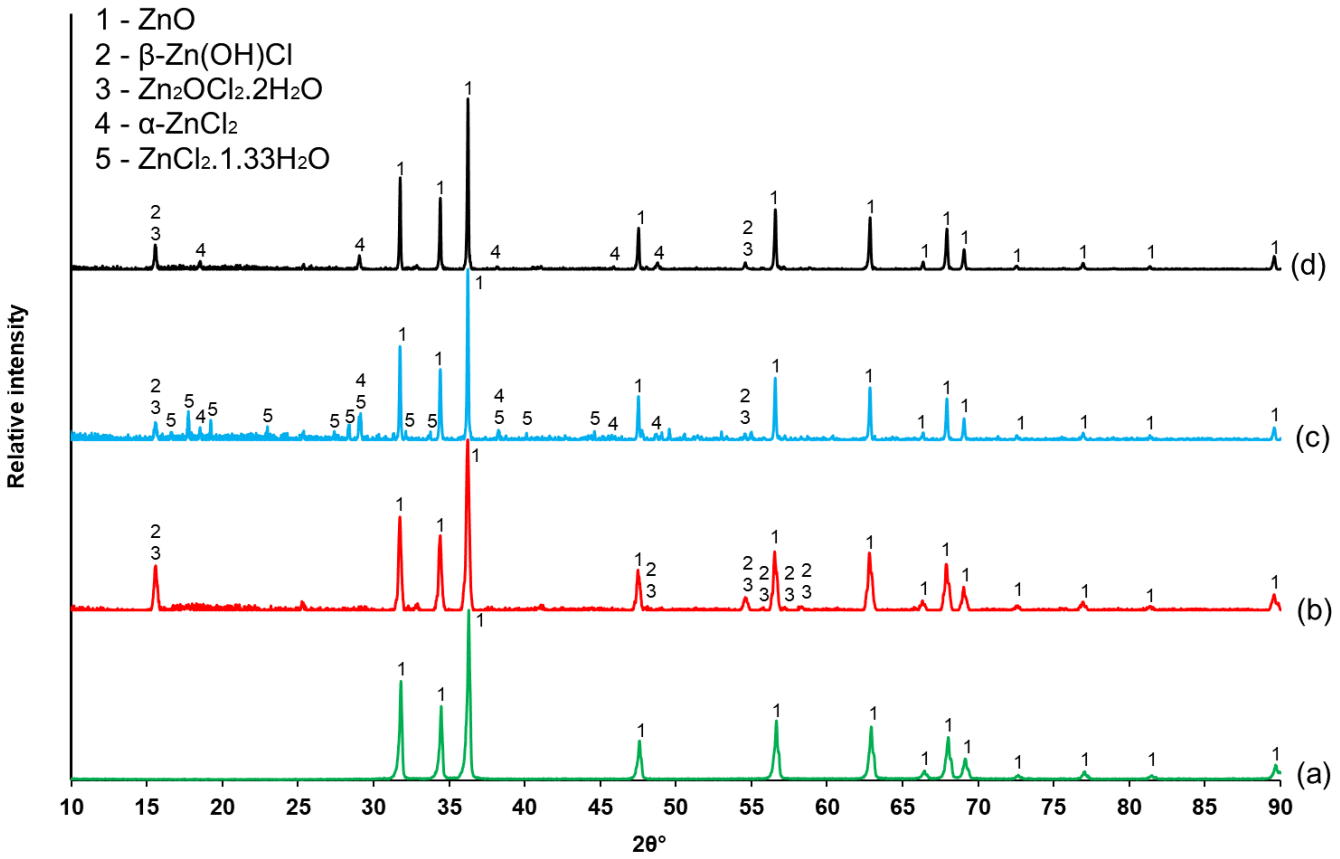

Figure 4: XRD pattern of ZnO (a), the post pyrolysis residue of ZPVC mixture at 200 (b), 230 (c), and 370 °C (d) all under nitrogen atmosphere.

SEM analysis was also utilised to confirm the association of both zinc and chlorine in the same crystal after the pyrolysis. Figure 5 shows hexagonal star crystals on a large ceramic fibre particle. These crystals are collected from the powder generated from the pyrolysis of the ZPVC mixture at 370 °C. EDS mapping confirms that these crystals contain both zinc and chlorine which suggests that they could be those of α-$ZnCl_2$.

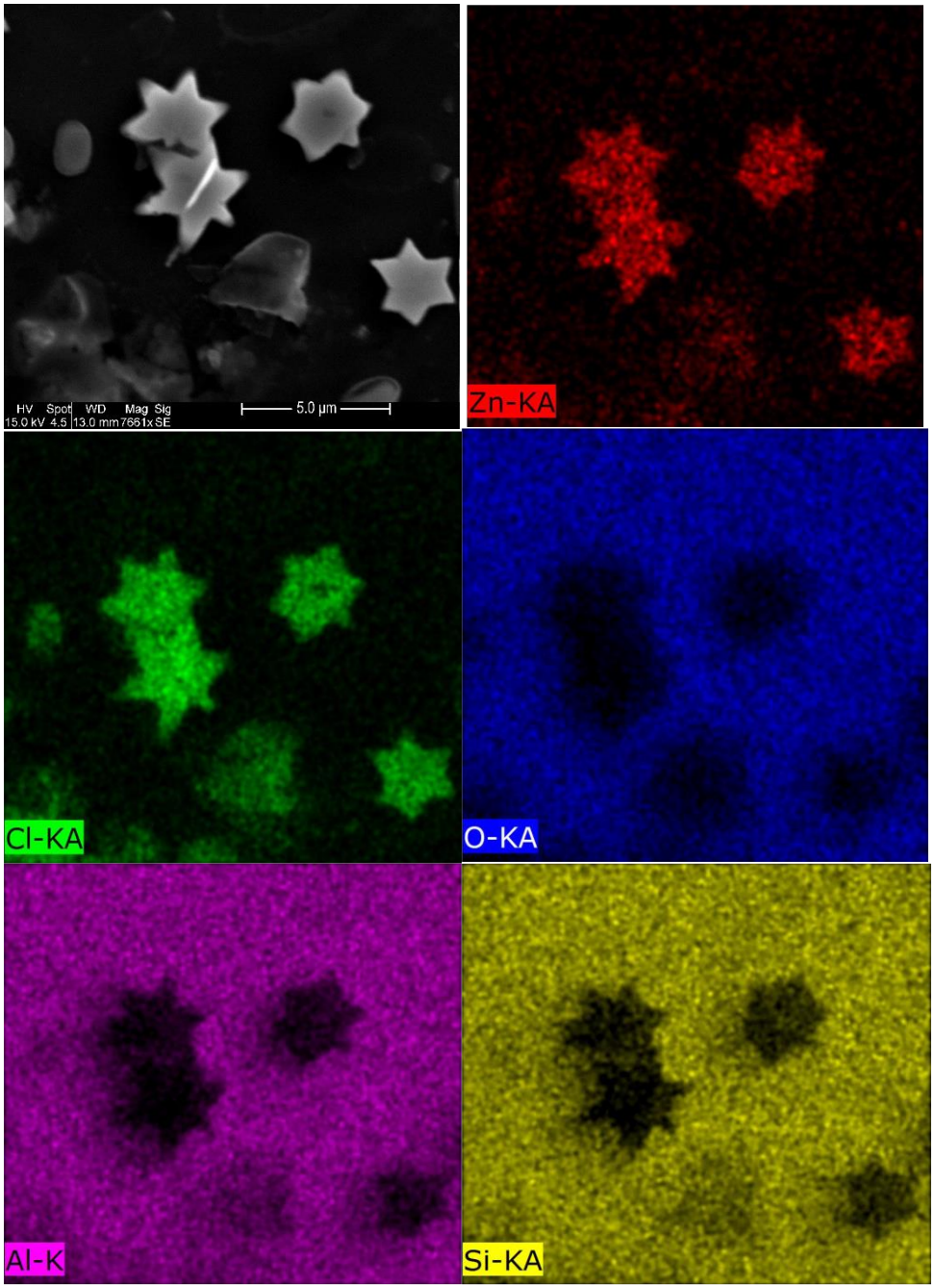

Figure 5: Secondary electron image of hexagonal star shaped crystals on a large ceramic fibre particle in a powder generated from the pyrolysis of ZPVC mixture under nitrogen at 370 °C.

Moreover, the formation of $ZnCl_2$ is also confirmed from the endothermic peak appearing in the temperature range 411 – 545 °C in Figure 2 which is attributed to its volatilisation into the gas phase. The endothermic peak appearing for ZPVC mixture is larger and sharper than that seen for pure PVC. The maximum heat flow is also slightly shifted to the right in the case of ZPVC showing a maximum evaporation rate at a temperature of about 503 °C which is in line with the high vapour pressure shown for $ZnCl_2$ in Figure 3 (b) with a value of 10 mmHg at 508

°C. This volatilisation behaviour is also in line with the thermodynamic analysis reported by Al-Harahsheh [7] and the TGA profile of pure $ZnCl_2$ reported by Jones et al. [55].

Two potential mechanistic pathways can be associated with the chlorination of ZnO:

1. Direct reaction of ZnO with hydrogen and chlorine in the PVC monomer.
2. Reaction of ZnO with the emitted gaseous HCl from PVC decomposition.

In the former case, the overall reaction can be written as in Equation 16, while in the latter, it is written as follows:

$$ZnO + 2HCl_{(g)} \rightarrow ZnCl_2 + H_2O \quad (15)$$

Evidence within literature suggests that the chlorination of ZnO is caused by a direct reaction with the PVC monomer [30, 47]. Zhang et al. [30] reported that the mass drop for ZPVC mixture started at a temperature of ~ 200 °C and that up to a temperature of about 271 °C, only H_2O fragments (from ZnO chlorination) were detected by the mass spectrometer with no evidence of HCl in the outlet stream. At temperatures slightly above 271 °C, HCl fragments started to appear [30]. Comparing that result with the data shown in Figure 3 (a) (10 K/min curve), it is clear that the third stage onset temperature is approximately 274 °C which is almost identical to the temperature reported in Zhang et al. [30]. This suggests that this stage is mainly associated with the evolution of HCl gas from the de-hydrochlorination of excess unreacted PVC. It is also clear that the heat flow signal (Figure 2) associated with the chlorination of ZnO rises significantly earlier than the endothermic one associated with pure PVC de-hydrochlorination. The XRD data in Figure 4 also shows that $Zn_2OCl_2.2H_2O$/β-Zn(OH)Cl phases form when the pyrolysis was done at 200 °C which is much lower than the onset temperature of pure PVC de-hydrochlorination; suggesting a direct interaction of ZnO with PVC. Data in the kinetics section 4.2.1 is also in favour of this conclusion.

Based on mineralogical data presented in Figure 4, the TGA/DTG profiles in Figure 3 (a), and the thermal behaviour of zinc oxy/hydroxide chloride species reported in literature [51-53], the following reaction sequence can be suggested for our reaction system based on starting and ceasing points of the DTG peaks of the ZPVC mixture:

1. Initial chlorine abstraction from PVC by ZnO (First DTG peak):

$$ZnO + 2(C_2H_3Cl)_n \rightarrow ZnCl_2 + 2(C_2H_2)_n + H_2O \quad (16)$$

2. Immediate capturing of formed H_2O and the simultaneous formation and decomposition of simonkolleite ($Zn_5(OH)_8Cl_2.H_2O$):

❖ Formation:

$$4ZnO + ZnCl_2 + 5H_2O \rightarrow Zn_5(OH)_8Cl_2.H_2O \quad (17)$$

❖ Decomposition (First DTG peak):

$$Zn_5(OH)_8Cl_2.H_2O \rightarrow \overbrace{2Zn(OH)Cl}^{detected\ by\ XRD} + 3ZnO + 4H_2O \qquad 206\ °C < T < 222\ °C \quad (18)$$

$$Zn_5(OH)_8Cl_2.H_2O \rightarrow \overbrace{Zn_2OCl_2.2H_2O}^{detected\ by\ XRD} + 3ZnO + 3H_2O \qquad 206\ °C < T < 222\ °C \quad (19)$$

3. Thermal decomposition of $Zn_2OCl_2.2H_2O$/β-Zn(OH)Cl (Second DTG peak):

$$2Zn(OH)Cl \rightarrow \overbrace{ZnCl_2}^{detected\ by\ XRD} + ZnO + H_2O \qquad 222\ °C < T < 260\ °C \quad (20)$$

$$Zn_2OCl_2.2H_2O \rightarrow \overbrace{ZnCl_2}^{detected\ by\ XRD} + ZnO + 2H_2O \qquad 222\ °C < T < 260\ °C \quad (21)$$

4. Excess unreacted PVC decomposition (Third DTG peak) (Reaction 12)

Following the sequence above, the DTG triplet in Figure 3 (a) can now be explained. The appearance of β-Zn(OH)Cl/$Zn_2OCl_2.2H_2O$ (Figure 4) at 370 °C, despite being reported to decompose completely at a lower temperature, might be explained by the reversible reaction

of ZnO with $ZnCl_2$ in presence of H_2O reported by Sorrell [52] and Garcia -Martinez et al. [53] at room temperature:

$$ZnCl_2 + ZnO + H_2O \leftrightarrows 2Zn(OH)Cl \quad (22)$$

The formation of zinc oxychloride was further confirmed by exposing a ZPVC residue generated at 370 °C to an open atmosphere for at least 6 hours, then analysing it using XRD (Figure 6). All the peaks in pattern (a) except one peak of ZnO at 36.4° completely disappeared, generating a new phase $Zn_5(OH)_8Cl_2.H_2O$ (simonkolleite). The zinc oxy/hydroxide chloride phases ($Zn_2OCl_2.2H_2O$/β-Zn(OH)Cl), however, are believed to form as intermediates prior to the formation of the $Zn_5(OH)_8Cl_2.H_2O$ phase. $ZnCl_2$ is a deliquescent material, which means that it is highly hygroscopic and tends to form in-situ acidic aqueous solutions. This results in the dissolution of ZnO in contact with it. The resultant solution then starts precipitating as $Zn_2OCl_2.2H_2O$/β-Zn(OH)Cl which finally transforms to $Zn_5(OH)_8Cl_2.H_2O$. Such result suggests that if the extraction of zinc is of interest, excess amount of PVC should be added to the mixture to chlorinate all ZnO, thus preventing the formation of the insoluble $Zn_5(OH)_8Cl_2.H_2O$ phase. Moreover, products generated from the pyrolysis of ZPVC should be protected from moisture to preserve the soluble $ZnCl_2$ crystals.

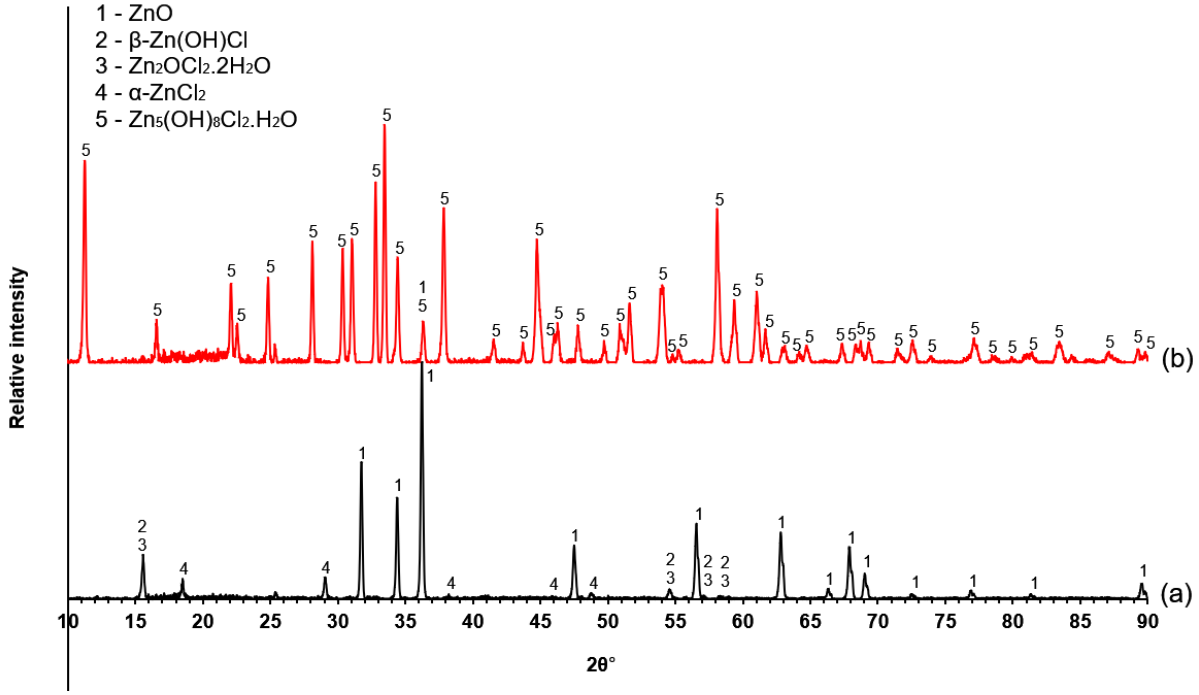

Figure 6: XRD pattern of the pyrolysis residue of ZPVC at 370 °C (a) and the same powder when exposed to the atmosphere for at least 6 hours (b).

The fourth mass loss in Figure 3 (a) is assigned to the simultaneous volatilisation of $ZnCl_2$ along with the thermal cracking of polyene structure; for 10 K/min curve, the loss is 28.5% where the thermal cracking accounts for 17.5% while the rest is related to $ZnCl_2$ volatilisation. The overall mass loss in that stage increases with increasing heating rate from 28.5% at 10 K/min to 37.9 and 41.7% at 30 and 50 K/min, respectively. This is attributed to the volatilisation of larger amounts of $ZnCl_2$ at higher heating rates which is in line with the percentages captured of HCl calculated earlier.

4.2. Non-isothermal kinetics

In the kinetics section, the mass loss in the temperature range 210 – 365 °C for pure PVC and ZPVC will be referred to as the "de-hydrochlorination" stage while the mass loss in the temperature range 390 – 550 °C will be referred to as "polyene thermal cracking" stage. Both the activation energy and the frequency factor calculated here represent apparent values that reflect the contribution of different processes occurring either sequentially or simultaneously.

Thus, their values will change with temperature/conversion due to the beginning or ceasing of chemical/physical events.

4.2.1. Kinetics of de-hydrochlorination stage for PVC and ZPVC

Figure 7 shows a sample of experimental data fitting for the de-hydrochlorination stage of pure PVC using FWO, KAS, and Friedman models. Slopes in Figure 7 were used to calculate the activation energy in the conversion range 0.1 – 0.9. Data fitting for obtaining the reaction model is also presented in Figure 7 (d). Compensation effect graphs for the estimation of the frequency factor are presented in the supplementary material (Figure S3).

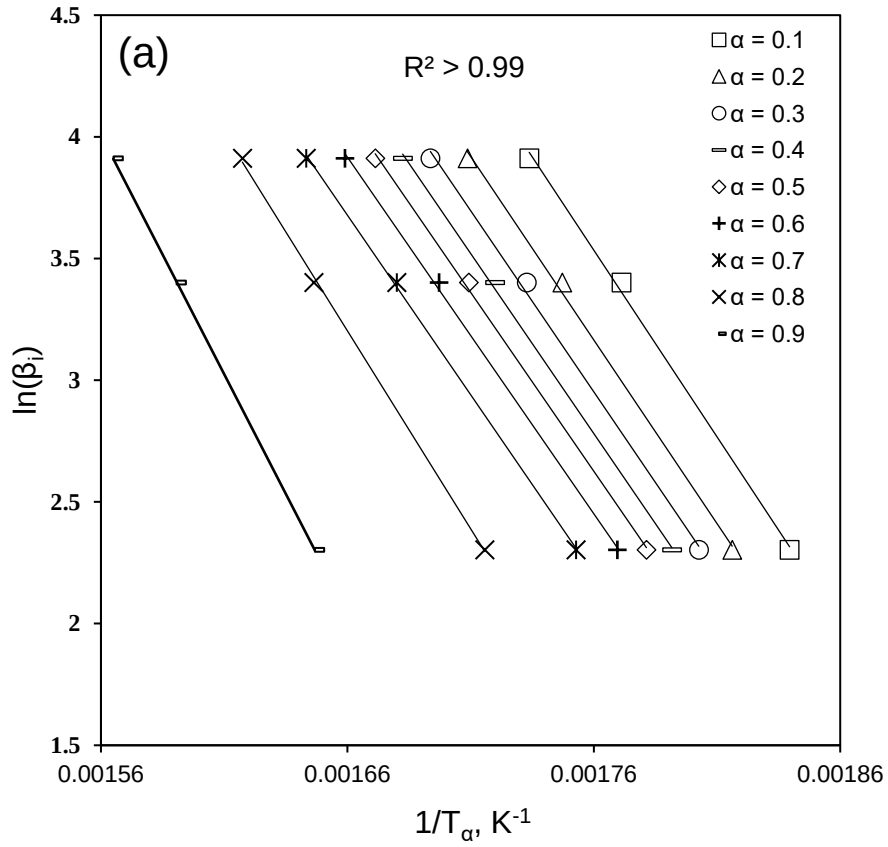
(a)
R² > 0.99
α = 0.1
α = 0.2
α = 0.3
α = 0.4
α = 0.5
α = 0.6
α = 0.7
α = 0.8
α = 0.9
ln(βi)
1/Tα, K-1
4.5
4
3.5
3
2.5
2
1.5
0.00156
0.00166
0.00176
0.00186

402

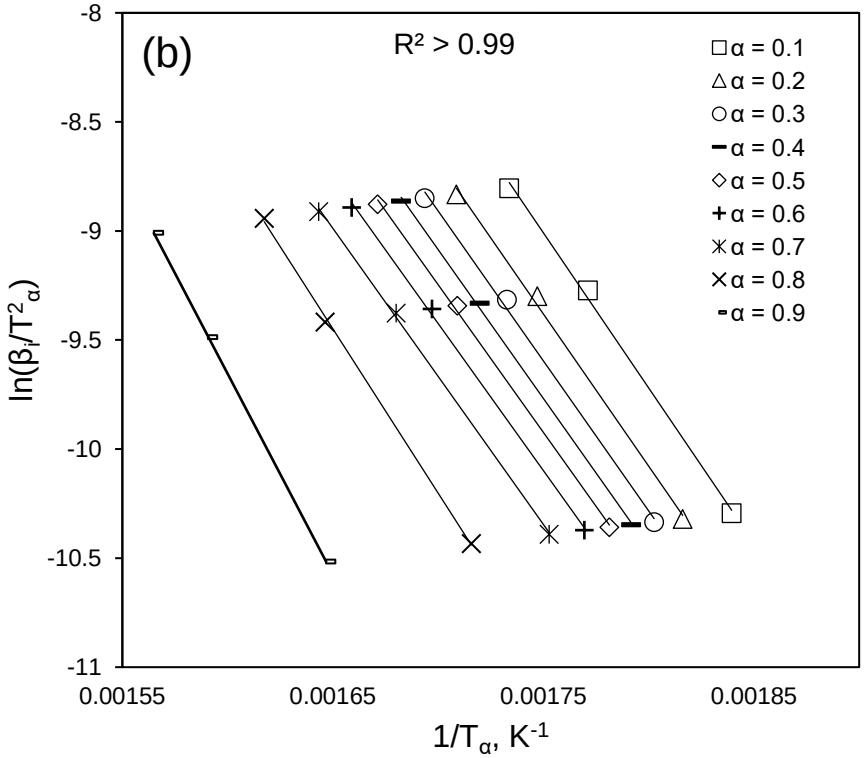
(b)
R² > 0.99
α = 0.1
α = 0.2
α = 0.3
α = 0.4
α = 0.5
α = 0.6
α = 0.7
α = 0.8
α = 0.9
ln(βi/T2α)
1/Tα, K-1
-8
-8.5
-9
-9.5
-10
-10.5
-11
0.00155
0.00165
0.00175
0.00185

403

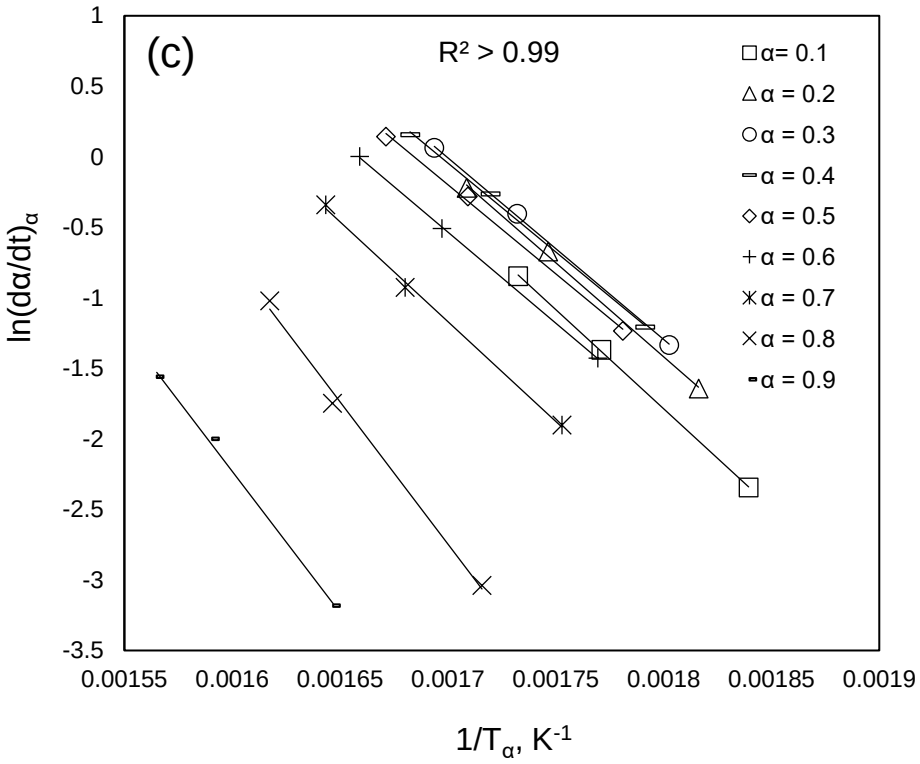

404

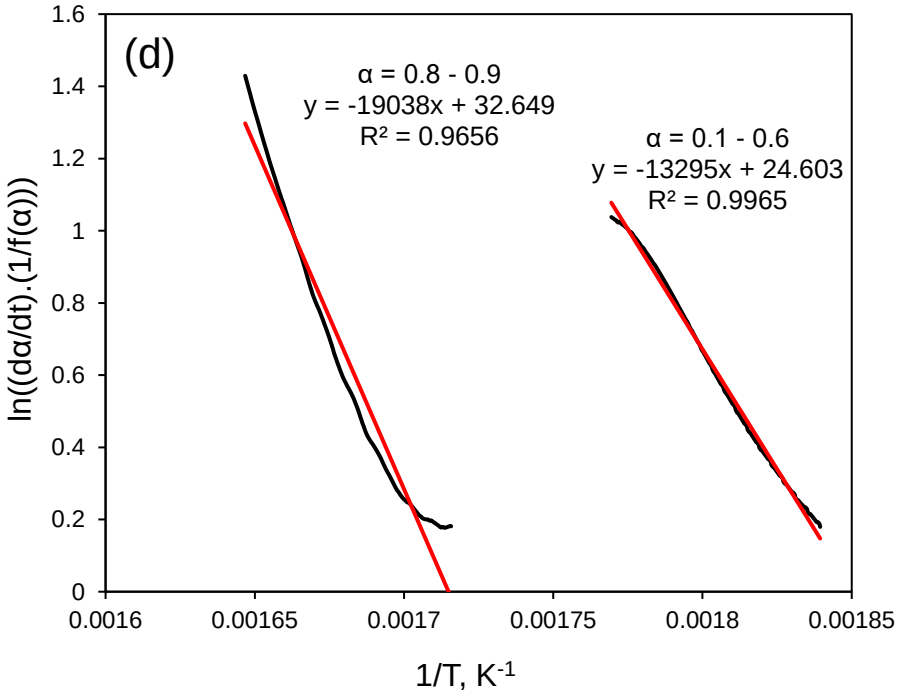

405
406 Figure 7: Experimental data fitting of the de-hydrochlorination stage of pure PVC using (a) FWO, (b) KAS and
407 (c) Friedman models for activation energy and (d) Linear model fitting for the prediction of the reaction model
408 $f(\alpha)$ (see Figure S4 in the supplementary material for other decomposition stages).

409 Table 1 shows the kinetic parameters for the de-hydrochlorination of pure PVC. The average

410 activation energy calculated using FWO, KAS and Friedman models are 123.1 ± 12.0, 119.8 ±

12.4 and 122.6 ± 24.2 kJ/mol, respectively. Values presented here are in good agreement with those reported in literature [44, 56, 57]. The activation energy does not change significantly with conversion until a conversion level of 0.7 is reached. This suggests that a single reaction mechanism controls the degradation in the conversion range 0.1 – 0.7. Above 0.7, the activation energy rises appreciably to a maximum of 153.2 kJ/mol at a conversion of 0.9 (KAS). It is also noticed that above a conversion level of 0.7, the degradation changes from being controlled by the reaction model $f(\alpha) = \alpha(1-\alpha)^{2.13}$ to a second order reaction model $f(\alpha) = (1-\alpha)^2$. Such behaviour might be attributed to the auto catalytic effect of PVC reported by Starnes and Ge [58]. In their work, they reported that the emitted HCl interacts with the formed polyene sequences to form polyenyl cation radicals leading to auto catalysis of de-hydrochlorination [58]. Thus, at high conversions (e.g., > 0.7), most of the emitted HCl will have already been swept by the purging gas resulting in lean amount of HCl in the vicinity of degrading PVC which makes further decomposition slow down, leading to high values of activation energy and an alteration in the reaction model. This also agrees with the fact that the used flow rate of nitrogen during the TGA runs was high (100 mL/min) which helps in sweeping emitted HCl at a faster rate.

Table 1: Kinetic parameters of de-hydrochlorination stage for pure PVC (first two stages in Figure 1).

Conversion, α	FWO		KAS		Friedman		Linear model fitting		
	Activation energy, kJ/mol	Frequency factor, ln(A)[a]	Activation energy, kJ/mol	Frequency factor, ln(A)[a]	Activation energy, kJ/mol	Frequency factor, ln(A)[a]	Activation energy, kJ/mol	Frequency factor, ln(A)[a]	*f(α)*
0.1	121.2	25.71	118.2	25.03	116.9	24.74	110.5	24.60	$\alpha(1-\alpha)^{2.13}$
0.2	119.2	25.26	116.0	24.53	110.9	23.37			
0.3	117.7	24.92	114.3	24.14	107.0	22.48			
0.4	117.0	24.76	113.5	23.96	104.8	21.98			
0.5	116.2	24.58	112.6	23.76	105.0	22.03			
0.6	115.8	24.48	112.1	23.64	107.3	22.55			
0.7	116.6	24.67	112.9	23.83	117.6	24.89	*Transition region (no fitting)*		
0.8	128.5	27.37	125.2	26.62	167.7	36.28	158.3	32.65	$(1-\alpha)^2$
0.9	155.4	33.49	153.2	32.99	166.6	36.03			
Average[b]	123.1 ± 12.0	26.14 ± 2.73	119.8 ± 12.4	25.39 ± 2.83	122.6 ± 24.2	26.04 ± 5.50	____		

a: Unit of A is min^{-1}.

b: Mean ± SD

Table 2: Kinetic parameters of de-hydrochlorination stage for ZPVC mixture (stages two and three in Figure 3 (a)).

Conversion, α	FWO		KAS		Friedman		Linear model fitting		
	Activation energy, kJ/mol	Frequency factor, ln(A)[a]	Activation energy, kJ/mol	Frequency factor, ln(A)[a]	Activation energy, kJ/mol	Frequency factor, ln(A)[a]	Activation energy, kJ/mol	Frequency factor, ln(A)[a]	*f(α)*
0.1	117.2	25.56	114.7	24.94	79.2	16.22	87.7	20.09	$\frac{1}{2}(1-\alpha)^3$
0.2	104.3	22.39	101.0	21.58	91.6	19.27			
0.3	101.3	21.65	97.7	20.76	92.0	19.36			
0.4	100.0	21.33	96.2	20.40	100.1	21.36			
0.5	105.0	22.56	101.3	21.65	122.9	26.96			
0.5	105.0	22.56	101.3	21.65	122.9	26.96	125.9	26.60	$1-\alpha$
0.6	116.2	25.31	113.0	24.53	147.5	33.01			
0.7	125.8	27.67	123.0	26.98	148.4	33.23			
0.8	131.1	28.98	128.4	28.31	127.7	28.14			
0.9	123.2	27.03	119.8	26.20	87.1	18.16			
Average[b]	113.8 ± 10.9	24.72 ± 2.67	110.6 ± 11.2	23.93 ± 2.75	110.7 ± 24.9	23.97 ± 6.13	____		

a: Unit of A is min^{-1}.
b: Mean ± SD

The addition of ZnO to PVC resulted in a change in the activation energy of the de-hydrochlorination stage (Table 2). The average activation energy over a conversion range of 0.1 – 0.9 changed from 119.8 ± 12.4 to 110.6 ± 11.2 kJ/mol when ZnO was added. To properly track the sequence of reactions, DTG and activation energy profiles were plotted against temperature for both PVC and ZPVC mixtures (Figure 8). Since the ZPVC mixture involves the decomposition of formed zinc oxy/hydroxide chlorides into solids (ZnO and $ZnCl_2$) and gaseous H_2O, the studied kinetic parameters will therefore be for sequential reactions. This means, the reported parameters will represent those related to the slowest step in the sequence. As mentioned earlier, the first DTG peak for ZPVC in Figure 8 (206 °C < T < 222 °C) is believed to be due to water evolution from the sequential ZnO chlorination (Reaction 16) followed by the formation/decomposition of $Zn_5(OH)_8Cl_2.H_2O$ (Reactions 17, 18 and 19). While these reactions are sequential, they could also proceed to a small extent in parallel due to possible incomplete reaction of emitted H_2O with $ZnCl_2$ and ZnO. The activation energies in the same temperature range for that peak compare very well with those related to pure PVC

de-hydrochlorination (Figure 8) which involves the scission of the C-Cl bond. This means, at that stage, the controlling mechanism could therefore be related to the chlorine abstraction from PVC by ZnO, while the decomposition of the hydroxide chloride ($Zn_5(OH)_8Cl_2.H_2O$) phase being the faster step. When the temperature increases to 230 °C (middle of second DTG peak of ZPVC), a drop in the activation energies can be seen to an average value of about 102.2 kJ/mol. This corresponds to a conversion range of 0.1 – 0.5, meaning that it is possible that a significant portion of the chlorine atoms in the PVC chain have been abstracted. This, in turn, would leave many chlorine atoms in the allylic position making their abstraction from PVC by ZnO more facile, and hence the drop in the activation energy (Figure 9). Rieche et al. [59] suggested that the charge separation in the C-Cl bond becomes accentuated when allylic sites are formed in the PVC chain. This would make the scission of this bond easier. Hence, for the second DTG peak of ZPVC, the controlling mechanism could be the decomposition of β-$Zn(OH)Cl/Zn_2OCl_2.2H_2O$ into ZnO, $ZnCl_2$ and gaseous H_2O. Such result is in agreement with the theoretical thermo-kinetic study performed by Ahmed et al. [54], where in their work the reported activation energy associated with the desorption of water from zinc oxychloride was 97.9 kJ/mol which compares well with the one reported here (102.2 kJ/mol). When the temperature reaches 262 °C, the activation energy starts rising to values comparable to those of pure PVC de-hydrochlorination (Figure 8). This is due to the fact that PVC in the ZPVC mixture starts to decompose normally into HCl and polyene. The similarity in the activation energy between ZPVC and PVC in the temperature range of 272 – 297 °C confirms what was suggested before by Zhang et al. [30] and Kosuda et al. [47] regarding the initial ZnO-PVC direct reaction and the subsequent normal PVC decomposition into HCl.

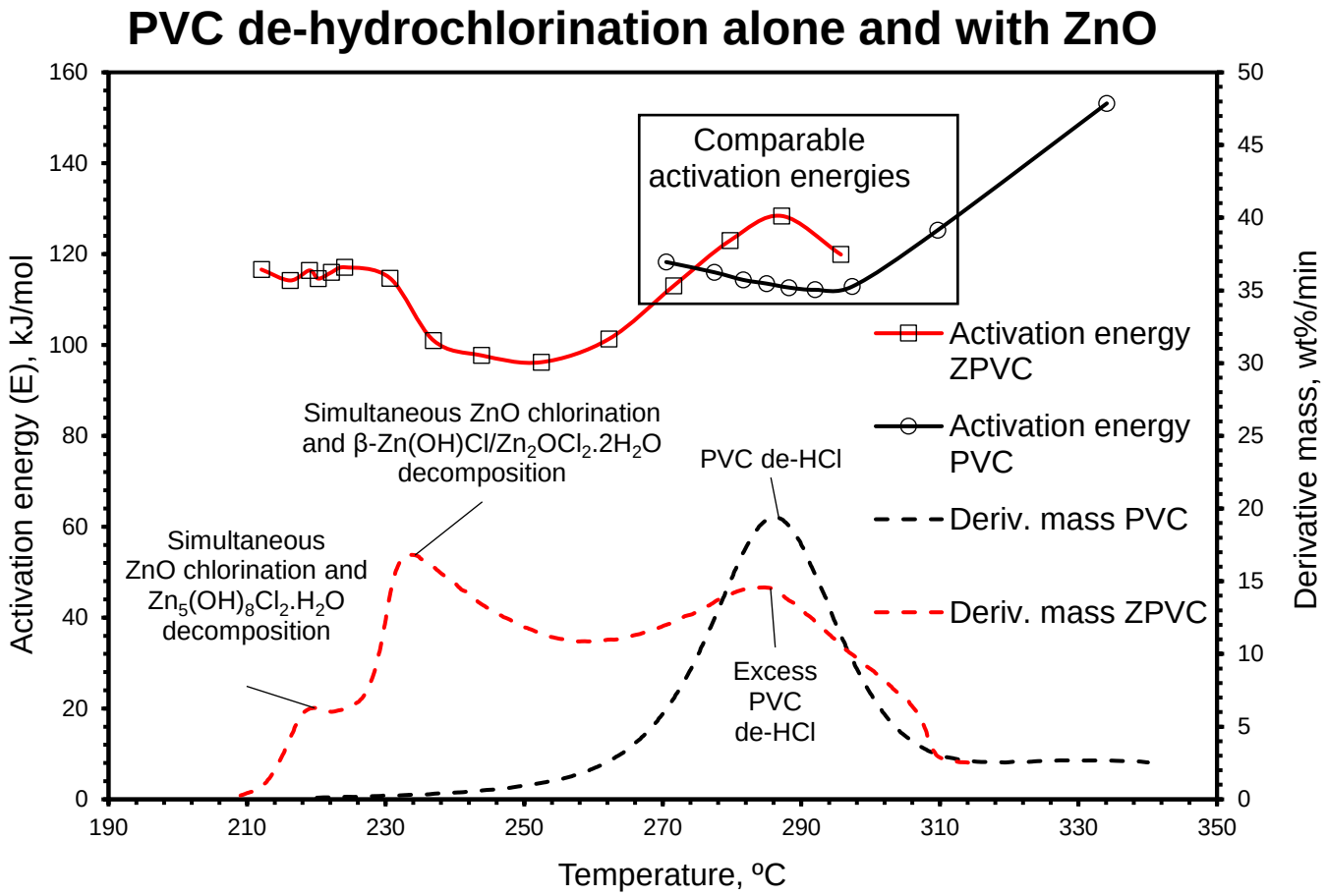

Figure 8: Activation energy and DTG profiles of the de-hydrochlorination stage in the case of ZPVC and PVC (activation energies were substituted from KAS model and all plots (including activation energy plots) were prepared based on 10 K/min profiles/data).

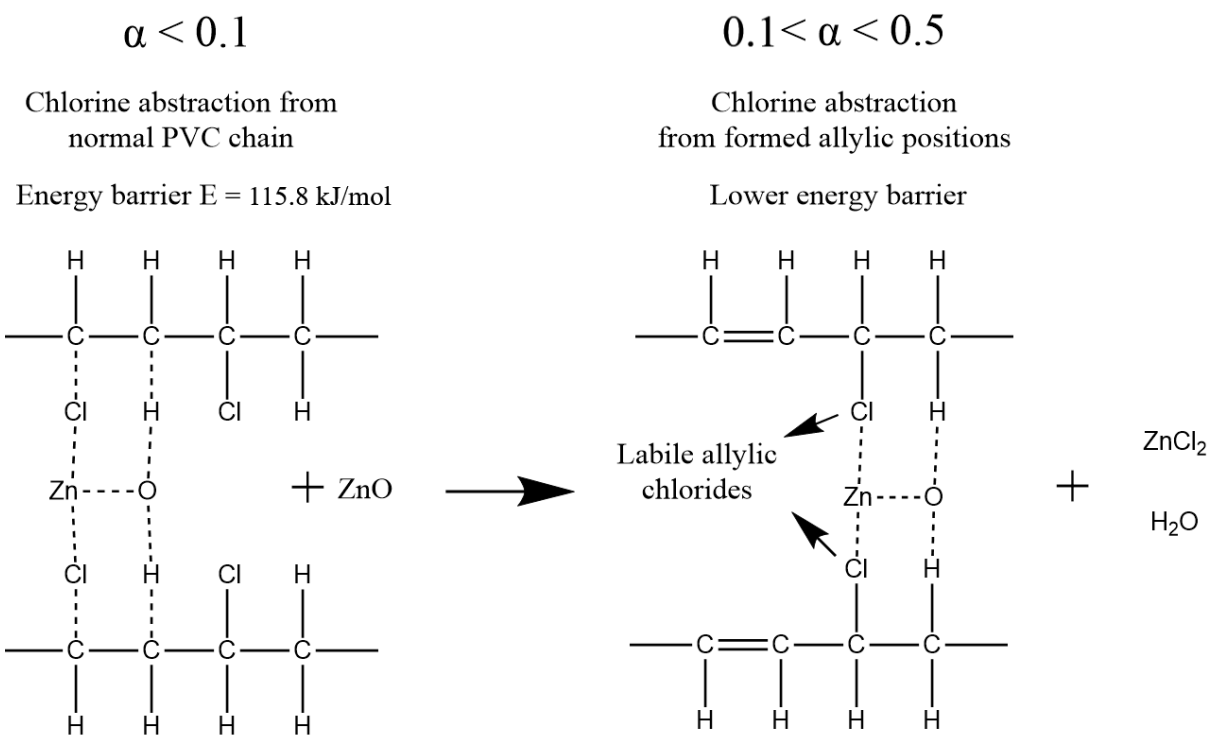

Figure 9: Possible formation of allylic chloride sites in the PVC chain by chlorine abstraction on ZnO.

4.2.2. Kinetics of polyene thermal cracking stage for PVC and ZPVC

Table 3 shows the kinetic parameters of the polyene thermal cracking in the case of pure PVC. Values of the activation energies for this stage are significantly higher than those related to de-hydrochlorination; values averaged over a conversion range 0.1 – 0.9 are 219.4 ± 16.4, 218.4 ± 17.7 and 205.8 ± 13.9 kJ/mol calculated using FWO, KAS and Friedman models, respectively.

Table 3: Kinetic parameters of polyene thermal cracking stage for pure PVC (third stage in Figure 1).

Conversion, α	FWO		KAS		Friedman		Linear model fitting		
	Activation energy, kJ/mol	Frequency factor, ln(A)[a]	Activation energy, kJ/mol	Frequency factor, ln(A)[a]	Activation energy, kJ/mol	Frequency factor, ln(A)[a]	Activation energy, kJ/mol	Frequency factor, ln(A)[a]	*f(α)*
0.1	254.6	41.28	256.2	41.56	226.7	36.37	201.8	31.67	$2(1-\alpha)^{\frac{3}{2}}$
0.2	235.4	37.90	235.7	37.95	211.1	33.62			
0.3	228.2	36.63	227.9	36.58	230.5	37.04			
0.4	220.4	35.26	219.6	35.12	192.6	30.36			
0.5	213.8	34.10	212.5	33.87	208.2	33.11			
0.6	210.4	33.50	208.8	33.21	200.0	31.66			
0.7	207.7	33.02	205.8	32.69	198.4	31.38			
0.8	204.6	32.47	202.4	32.09	195.4	30.85			
0.9	199.9	31.65	197.2	31.17	189.0	29.73			
Average[b]	219.4 ± 16.4	35.09 ± 2.89	218.4 ± 17.7	34.92 ± 3.11	205.8 ± 13.9	32.68 ± 2.45	_____		

a: Unit of A is min^{-1}.
b: Mean ± SD.

Table 4: Kinetic parameters of polyene thermal cracking stage for ZPVC mixture (fourth stage in Figure 3 (a)).

Conversion, α	FWO		KAS		Friedman		Linear model fitting		
	Activation energy, kJ/mol	Frequency factor, ln(A)[a]	Activation energy, kJ/mol	Frequency factor, ln(A)[a]	Activation energy, kJ/mol	Frequency factor, ln(A)[a]	Activation energy, kJ/mol	Frequency factor, ln(A)[a]	*f(α)*
0.1	115.3	16.38	109.3	15.36	97.5	13.34	101.2	13.82	$\frac{3}{2}(1-\alpha)^{\frac{1}{3}}$
0.2	104.3	14.50	97.2	13.29	71.6	8.92			
0.3	95.5	13.00	87.7	11.67	70.1	8.66			
0.4	92.7	12.52	84.5	11.12	80.0	10.35			
0.5	92.7	12.52	84.4	11.10	87.2	11.58			
0.6	93.2	12.61	84.7	11.16	85.1	11.22			
0.7	92.5	12.49	83.9	11.02	73.2	9.19			
0.8	88.8	11.86	79.8	10.32	45.6	4.47			
0.9	83.5	10.95	74.0	9.33	66.4	8.03	Did not fit in the model		
Average[b]	95.4 ± 8.7	12.98 ± 1.49	87.3 ± 9.7	11.60 ± 1.66	75.2 ± 14.0	9.53 ± 2.39	_____		

a: Unit of A is min^{-1}.
b: Mean ± SD.

A drop in the values of the activation energy is observed as the reaction progresses further. This might be attributed to the fact that the polyene thermal cracking stage involves the evolution of different hydrocarbons [46]. This, in turn, may lead to the formation of separate transition states at different conversion levels based on the structure of the formed hydrocarbon, which then leads to a continuous change in the activation energy barrier with conversion. Despite the variation of the activation energy with conversion, a single reaction model was able to fit the experimental data in the conversion range of 0.1 – 0.9. The reaction model suggests that the decomposition is chemical reaction controlled throughout the stage with a reaction order of $\frac{3}{2}$ (Table 3).

Table 4 reports the kinetic parameters of the polyene thermal cracking stage for the ZPVC mixture. Figure 3 (b) as well as the thermodynamics analysis reported in Al-Harahsheh [7] and the TGA profile for $ZnCl_2$ presented in Jones et al. [55] suggest that $ZnCl_2$ volatilises in the temperature range of 400 – 520 °C. This means that the reported kinetic parameters in Table 4 represent apparent values from simultaneous polyene thermal cracking and volatilisation of $ZnCl_2$. The activation energy dropped considerably from 218.4 ± 17.7 kJ/mol in the case of pure PVC (Table 3) to 87.3 ± 9.7 kJ/mol in the case of ZPVC mixture. Such a drop can be attributed to the contribution of the volatilisation of $ZnCl_2$ on the apparent activation energy. This is because physical processes, in general, are known to exhibit significantly lower activation energies compared to chemical ones. Thus, the overall calculated activation energy significantly decreased. The overall process was able to be described by one reaction model with a reaction order of $\frac{1}{3}$.

The importance of the data reported in this work lies in the fact that there is a significant variation in the chemistry of EAFD world-wide which depends on the followed smelting practices and the type of the feeding materials to EAFs. In fact, further studies on the effect of other important minerals in EAFD such Fe_2O_3, Fe_3O_4, $ZnFe_2O_4$, and PbO on the decomposition

kinetics of PVC should be done. Such studies on the interaction between PVC and other metal oxides allow the prediction of the process kinetics and the appropriate holding temperatures for best process economics for different EAFDs with different chemistries (i.e., EAFD from different sources/countries). Thus, for future work, we believe other deep kinetics investigations on the effect of other EAFD constituents (mentioned earlier) on PVC degradation should be considered.

5 Conclusions

This work studied the kinetics and the behaviour of PVC thermal decomposition in the presence of a stoichiometric quantity of ZnO. Apparent activation energy, frequency factor, and the reaction model were extracted based on non-isothermal study of thermogravimetric scans at 10, 30, and 50 K/min under inert environment. The following conclusions are made:

- The TGA data suggests an excellent chlorine fixing ability of ZnO such that when a stoichiometric amount of ZnO was added (39.4 wt%), the percentage of HCl captured was ~ 28.9, 42.6 and 46.3% at heating rates of 10, 30 and 50 K/min, respectively.
- The formation of water soluble zinc chloride is clearly seen in the SEM and XRD scans suggesting that PVC can be incorporated with metallurgical wastes such as EAFD for the extraction of metallic zinc through water leaching of the post pyrolysis residue.
- It is recommended that an excess PVC amount is used in the co-thermal treatment with ZnO containing wastes (such as EAFD) to completely chlorinate this constituent, thus preventing the formation of the insoluble $Zn_5(OH)_8Cl_2.H_2O$ (Simonkolleite) phase.
- A noticeable change in the activation energy of PVC de-hydrochlorination was witnessed when ZnO was added. The variation of the activation energy with temperature suggested different controlling mechanisms at different conversion ranges

between chlorine abstraction and thermal decomposition of zinc oxy/hydroxide chloride species.

- ZnO can be categorised as an active catalyst for PVC de-hydrochlorination decreasing its onset decomposition temperature from 272 to 214 °C.
- It is suggested that ZnO initially abstracts chlorine from PVC to form $ZnCl_2$ which then reacts with ZnO and emitted H_2O to form the oxy/hydroxide chloride species $Zn_2OCl_2.2H_2O$/β-Zn(OH)Cl. These phases then start to decompose at temperatures above 222 °C into $ZnCl_2$, ZnO and H_2O.
- A significant drop in the activation energy of polyene thermal cracking was seen when ZnO was added which might be assigned to the physical contribution of the volatilisation of formed $ZnCl_2$ in that temperature range.

References

[1] M. Al-Harahsheh, A. Al-Otoom, L. Al-Makhadmah, I.E. Hamilton, S. Kingman, S. Al-Asheh, M. Hararah, Pyrolysis of poly(vinyl chloride) and—electric arc furnacedust mixtures, Journal of Hazardous Materials, 299 (2015) 425-436.

[2] P. Oustadakis, P.E. Tsakiridis, A. Katsiapi, S. Agatzini-Leonardou, Hydrometallurgical process for zinc recovery from electric arc furnace dust (EAFD): Part I: Characterization and leaching by diluted sulphuric acid, Journal of Hazardous Materials, 179 (2010) 1-7.

[3] U. Brandner, J. Antrekowitsch, M. Leuchtenmueller, A review on the fundamentals of hydrogen-based reduction and recycling concepts for electric arc furnace dust extended by a novel conceptualization, International Journal of Hydrogen Energy, (2021).

[4] J. Madias, Electric Furnace Steelmaking, in: Treatise on Process Metallurgy, 2014, pp. 271-300.

[5] G.-S. Lee, Y.J. Song, Recycling EAF dust by heat treatment with PVC, Minerals engineering, 20 (2007) 739-746.

[6] N. Tsubouchi, H. Hashimoto, N. Ohtaka, Y. Ohtsuka, Chemical characterization of dust particles recovered from bag filters of electric arc furnaces for steelmaking: Some factors influencing the formation of hexachlorobenzene, Journal of hazardous materials, 183 (2010) 116-124.

[7] M. Al-Harahsheh, Thermodynamic Analysis on the Thermal Treatment of Electric Arc Furnace Dust-PVC Blends, Arabian Journal for Science and Engineering, (2017) 1-13.

[8] T. Havlik, B. Friedrich, S. Stopic, Pressure leaching of EAF dust with sulphuric acid, Erzmetall, 57 (2004) 83-90.

[9] T. Havlik, M. Turzakova, S. Stopic, B. Friedrich, Atmospheric leaching of EAF dust with diluted sulphuric acid, Hydrometallurgy, 77 (2005) 41-50.

[10] A.J.B. Dutra, P.R.P. Paiva, L.M. Tavares, Alkaline leaching of zinc from electric arc furnace steel dust, Minerals Engineering, 19 (2006) 478-485.

[11] L.A. Al-Makhadmeh, M.A. Batiha, M.S. Al-Harahsheh, I.S. Altarawneh, S.E. Rawadieh, The Effectiveness of Zn Leaching from EAFD Using Caustic Soda, Water, Air, & Soil Pollution, 229 (2018) 33.

[12] M. Morcali, O. Yucel, A. Aydin, B. Derin, Carbothermic reduction of electric arc furnace dust and calcination of waelz oxide by semi-pilot scale rotary furnace, Journal of Mining and Metallurgy B: Metallurgy, 48 (2012) 173-184.

[13] T. Suetens, B. Klaasen, K. Van Acker, B. Blanpain, Comparison of electric arc furnace dust treatment technologies using exergy efficiency, Journal of cleaner production, 65 (2014) 152-167.

[14] H.-n. Zhang, J.-l. Li, A.-j. Xu, Q.-x. Yang, D.-f. He, N.-y. Tian, Carbothermic reduction of zinc and iron oxides in electric arc furnace dust, Journal of iron and steel research international, 21 (2014) 427-432.

[15] M. Cruells, A. Roca, C. Núñez, Electric arc furnace flue dusts: characterization and leaching with sulphuric acid, Hydrometallurgy, 31 (1992) 213-231.

[16] V. Montenegro, P. Oustadakis, P.E. Tsakiridis, S. Agatzini-Leonardou, Hydrometallurgical treatment of steelmaking electric arc furnace dusts (EAFD), Metallurgical and Materials Transactions B, 44 (2013) 1058-1069.

[17] F. Kukurugya, T. Vindt, T. Havlík, Behavior of zinc, iron and calcium from electric arc furnace (EAF) dust in hydrometallurgical processing in sulfuric acid solutions: Thermodynamic and kinetic aspects, Hydrometallurgy, 154 (2015) 20-32.

[18] Y.Y. Teo, H.S. Lee, Y.C. Low, S.W. Choong, K.O. Low, Hydrometallurgical extraction of zinc and iron from electric arc furnace dust (EAFD) using hydrochloric acid, Journal of Physical Science, 29 (2018) 49-54.

[19] M.A. Keane, Catalytic conversion of waste plastics: focus on waste PVC, Journal of Chemical Technology & Biotechnology: International Research in Process, Environmental & Clean Technology, 82 (2007) 787-795.

[20] J. Yu, L. Sun, C. Ma, Y. Qiao, H. Yao, Thermal degradation of PVC: A review, Waste Management, 48 (2016) 300-314.

[21] Ceresana-Research, Additives for polymers, (2014) pp. 10–11.

[22] M. Al-Harahsheh, J. Al-Nu'airat, A. Al-Otoom, H. Al-jabali, M. Al-zoubi, Treatments of electric arc furnace dust and halogenated plastic wastes: A review, Journal of Environmental Chemical Engineering, (2018) 102856.
[23] I. Mersiowsky, R. Stegmann, J. Ejlertsson, Long term behaviour of poly (vinyl chloride) products under soil buried and landfill conditions, Plastics, rubber and composites, 28 (1999) 321-326.
[24] J.C. Wagner, A.E. Green, Correlation of chlorinated organic compound emissions from incineration with chlorinated organic input, Chemosphere, 26 (1993) 2039-2054.
[25] T. Katami, A. Yasuhara, T. Okuda, T. Shibamoto, Formation of PCDDs, PCDFs, and coplanar PCBs from polyvinyl chloride during combustion in an incinerator, Environmental science & technology, 36 (2002) 1320-1324.
[26] M. Al-harahsheh, S. Kingman, L. Al-Makhadmah, I.E. Hamilton, Microwave treatment of electric arc furnace dust with PVC: Dielectric characterization and pyrolysis-leaching, Journal of Hazardous Materials, 274 (2014) 87-97.
[27] M. Al-Harahsheh, Y. Orabi, S. Al-Asheh, Comparative study on the pyrolysis and leachability of washed/unwashed electric arc furnace dust-PVC mixtures and their residues, Journal of Environmental Chemical Engineering, (2021) 105410.
[28] Y. Masuda, T. Uda, O. Terakado, M. Hirasawa, Pyrolysis study of poly (vinyl chloride)–metal oxide mixtures: quantitative product analysis and the chlorine fixing ability of metal oxides, Journal of Analytical and Applied Pyrolysis, 77 (2006) 159-168.
[29] A. Ballistreri, S. Foti, P. Maravigna, G. Montaudo, E. Scamporrino, Effect of metal oxides on the evolution of aromatic hydrocarbons in the thermal decomposition of PVC, Journal of Polymer Science: Polymer Chemistry Edition, 18 (1980) 3101-3110.
[30] B. Zhang, X.-Y. Yan, K. Shibata, T. Uda, M. Tada, M. Hirasawa, Thermogravimetric-mass spectrometric analysis of the reactions between oxide (ZnO, Fe2O3 or ZnFe2O4) and polyvinyl chloride under inert atmosphere, Materials Transactions, JIM, 41 (2000) 1342-1350.
[31] H.E. Kissinger, Reaction kinetics in differential thermal analysis, Analytical chemistry, 29 (1957) 1702-1706.
[32] H.L. Friedman, Kinetics of thermal degradation of char-forming plastics from thermogravimetry. Application to a phenolic plastic, in: Journal of polymer science part C: polymer symposia, Wiley Online Library, 1964, pp. 183-195.
[33] T. Ozawa, A new method of analyzing thermogravimetric data, Bulletin of the chemical society of Japan, 38 (1965) 1881-1886.
[34] J.H. Flynn, L.A. Wall, General treatment of the thermogravimetry of polymers, Journal of Research of the National Bureau of Standards. Section A, Physics and Chemistry, 70 (1966) 487.
[35] T. Akahira, T. Sunose, Res. Report Chiba Inst. Technol, Sci. Technol, 16 (1971) 22.
[36] A. Altomare, N. Corriero, C. Cuocci, A. Falcicchio, A. Moliterni, R. Rizzi, QUALX2. 0: a qualitative phase analysis software using the freely available database POW_COD, Journal of Applied Crystallography, 48 (2015) 598-603.
[37] J. Šesták, G. Berggren, Study of the kinetics of the mechanism of solid-state reactions at increasing temperatures, Thermochimica Acta, 3 (1971) 1-12.
[38] S. Vyazovkin, A.K. Burnham, J.M. Criado, L.A. Pérez-Maqueda, C. Popescu, N. Sbirrazzuoli, ICTAC Kinetics Committee recommendations for performing kinetic computations on thermal analysis data, Thermochimica acta, 520 (2011) 1-19.
[39] A.W. Coats, J. Redfern, Kinetic parameters from thermogravimetric data, Nature, 201 (1964) 68-69.
[40] S. Vyazovkin, N. Sbirrazzuoli, Isoconversional kinetic analysis of thermally stimulated processes in polymers, Macromolecular Rapid Communications, 27 (2006) 1515-1532.
[41] S. Vyazovkin, Isoconversional kinetics, in: Handbook of thermal analysis and calorimetry, Elsevier, 2008, pp. 503-538.
[42] C. Doyle, Estimating isothermal life from thermogravimetric data, Journal of Applied Polymer Science, 6 (1962) 639-642.

[43] S. Vyazovkin, Determining Preexponential Factor in Model-Free Kinetic Methods: How and Why?, Molecules, 26 (2021) 3077.
[44] A. Marcilla, M. Beltrán, Thermogravimetric kinetic study of poly(vinyl chloride) pyrolysis, Polymer Degradation and Stability, 48 (1995) 219-229.
[45] S.C. Oh, W.-T. Kwon, S.-R. Kim, Dehydrochlorination characteristics of waste PVC wires by thermal decomposition, Journal of Industrial and Engineering Chemistry, 15 (2009) 438-441.
[46] M. Blazso, E. Jakab, Effect of metals, metal oxides, and carboxylates on the thermal decomposition processes of poly (vinyl chloride), Journal of Analytical and Applied Pyrolysis, 49 (1999) 125-143.
[47] T. Kosuda, T. Okada, S. Nozaka, Y. Matsuzawa, T. Shimizu, S. Hamanaka, S. Mishima, Characteristics and mechanism of low temperature dehydrochlorination of poly (vinyl chloride) in the presence of zinc (II) oxide, Polymer degradation and stability, 97 (2012) 584-591.
[48] D.W. Green, R.H. Perry, Perry's Chemical Engineers' Handbook, Eighth Edition, McGraw-Hill Education, 2007.
[49] H. Tanaka, A. Fujioka, Influence of thermal treatment on the structure and adsorption properties of layered zinc hydroxychloride, Materials Research Bulletin, 45 (2010) 46-51.
[50] A. Moezzi, M. Cortie, A. McDonagh, Transformation of zinc hydroxide chloride monohydrate to crystalline zinc oxide, Dalton Transactions, 45 (2016) 7385-7390.
[51] O. Srivastava, E. Secco, Studies on metal hydroxy compounds. I. Thermal analyses of zinc derivatives ε-Zn (OH) 2, Zn5 (OH) 8Cl2. H2O, β-ZnOHCl, and ZnOHF, Canadian Journal of Chemistry, 45 (1967) 579-583.
[52] C.A. Sorrell, Suggested chemistry of zinc oxychloride cements, Journal of the American Ceramic Society, 60 (1977) 217-220.
[53] O. Garcia-Martinez, E. Vila, J.M. de Vidales, R. Rojas, K. Petrov, On the thermal decomposition of the zinc (II) hydroxide chlorides Zn 5 (OH) 8 Cl 2· H 2 O and β-Zn (OH) Cl, Journal of Materials Science, 29 (1994) 5429-5434.
[54] O.H. Ahmed, M. Altarawneh, M. Al-Harahsheh, Z.-T. Jiang, B.Z. Dlugogorski, Recycling of zincite (ZnO) via uptake of hydrogen halides, Physical Chemistry Chemical Physics, 20 (2018) 1221-1230.
[55] F. Jones, H. Tran, D. Lindberg, L. Zhao, M. Hupa, Thermal stability of zinc compounds, Energy & fuels, 27 (2013) 5663-5669.
[56] S. Kim, Pyrolysis kinetics of waste PVC pipe, Waste management, 21 (2001) 609-616.
[57] G. Sivalingam, R. Karthik, G. Madras, Effect of metal oxides on thermal degradation of poly (vinyl acetate) and poly (vinyl chloride) and their blends, Industrial & engineering chemistry research, 42 (2003) 3647-3653.
[58] W.H. Starnes, X. Ge, Mechanism of autocatalysis in the thermal dehydrochlorination of poly (vinyl chloride), Macromolecules, 37 (2004) 352-359.
[59] A. Rieche, A. Grimm, H. Mücke, Untersuchungen über Stabilität von Suspensions-PVC, Kunststoffe, 52 (1962) 265-268.